Arch. Metall. Mater. **66** (2021), 3, 847-851

DOI: 10.24425/amm.2021.136389

CANDAN SEN ELKOCA[1*], BULENT EKMEKCI[2], OKTAY ELKOCA[3]

A STUDY ON THE SURFACE ROUGHNESS OF GALVANNEALED LOW CARBON Al-KILLED AND Ti-Nb STABILIZED INTERSTITIAL FREE STEELS

In this study, the surface roughness of galvannealed low carbon Al-killed and Ti-Nb stabilized interstitial free steels was investigated using the industrial galvannealing process parameters. The iron content of the coatings was also analysed to establish a relationship with the surface roughness and coating composition.

The surface roughness displayed an exponential behaviour with increasing of annealing time at each annealing temperature in both steel coatings, which was in an increasing order in the galvannealed low carbon Al-killed steel coating, whereas it was a reverse order in the galvannealed Ti-Nb stabilized interstitial free steel coating. The craters were observed on the galvannealed coatings resulting in high surface roughness. Increasing the iron content of the coatings leads to a reduction in the surface roughness with δ_{1k} phase.

Keywords: Galvannealing, galvannealed steel, hot-dip galvanizing, Fe-Zn phases, surface roughness

1. Introduction

Galvannealing is a diffusion process for producing an iron-zinc alloy coated also known as galvannealed steel by heating the hot-dip galvanized steel. The galvannealed steels offer several advantages over regular hot-dip galvanized coatings: better paintability, improved spot-welding characteristics, and increased corrosion resistance in the painted condition [1-4]. Because of these favourable properties, galvannealed steel has gained increasing use in the automotive industry. The growing importance of galvannealed coatings has led to many research studies on analysing their properties and evolution. Cold-rolled steel is first continuously hot-dipped in a molten zinc bath at around 460°C to produce an unalloyed zinc coating (Fig. 1). Upon exiting the bath, the zinc coating is subjected to an in-line annealing heat treatment at around 520°C, which converts zinc coating to an alloy coating of Fe-Zn intermetallic compounds. The coating layer on a galvannealed steel usually consists of five intermetallic compounds, Γ (Fe_3Zn_{10}), Γ_1 ($Fe_{11}Zn_{40}$), δ_{1k} ($FeZn_7$), δ_{1p} ($FeZn_{10}$), and ζ ($FeZn_{13}$) phases in the decreasing order of the iron content, according to the Fe-Zn binary phase diagram [5-8].

The properties of galvannealed coatings largely depend on Fe-Zn reaction kinetics, associated with the alloy content of zinc bath, chemical composition, microstructure, and surface condition of the steel substrate [9-12]. It is not easy to control the evolution of Fe-Zn phases in a galvannealed coating since they grow quite rapidly through the heat activation induced by the galvannealing process. In the industrial manufacturing pro-

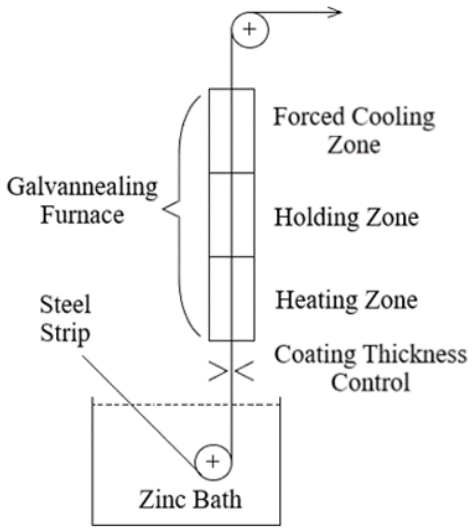

Fig. 1. Schematic diagram of an industrial galvannealing process

[1] BULENT ECEVIT UNIVERSITY, ALAPLI VOCATIONAL HIGH SCHOOL, ZONGULDAK 67850, TURKEY
[2] BULENT ECEVIT UNIVERSITY, DEPARTMENT OF MECHANICAL ENGINEERING, ZONGULDAK 67100, TURKEY
[3] DUZCE UNIVERSITY, DEPARTMENT OF MECHANICAL ENGINEERING, DUZCE 81620, TURKEY

* Corresponding author: candansen@gmail.com

cess, annealing time and temperature are the primary process parameters considering the reaction kinetics of Fe-Zn phases, which requires fast feedback to the operating system to adjust coating properties.

The surface roughness as a surface property of the galvannealed coatings influences the forming process of galvannealed steels since it alters the deformation behaviour by changing friction between the coating and die [13]. Sriram et al. [13] reported that cubic delta (δ_{1k}) coatings with lower roughness had better formability than rod delta coatings (δ_{1p}). Additionally, a good correlation was found between the index of image clarity after painting and galvannealed surfaces [14]. The surface roughness of a galvannealed steel can be measured manually and intermittently with a portable contact profiler on the line [15] or continuously using a non-contact profiler in-line [16]. These measurements can also be entered into the operating system as quick feedback either manually or online, depending on the measurement method for adjusting galvannealing parameters during actual production runs.

No detailed study has been found to put forward the surface roughness of the galvannealed coatings produced through an industrial galvannealing process. This study elucidates the surface microstructures forming surface roughness during the galvannealing process and establish relations between surface roughness, galvannealing process parameters, and coating iron content.

2. Experimental Procedure and Materials

The sample sheets of zinc-coated low carbon Al-killed steel (AKS) and Ti-Nb stabilized interstitial free steel (IFS) were received from a continuous hot-dip galvanizing line with an induction heating unit to produce galvannealed coatings. The AKS and IFS sheets were first dipped into a liquid zinc bath containing 0.10 wt.% Al at 460°C in the line and then withdrawn from the bath. The zinc-coated samples were taken at the exit of the galvanizing line from the regions close to the welding line, where the tail and head ends of the steel strips are welded. No alloying occurs in this region in practice because the induction heating unit in the line automatically shuts off when this part of the advancing steel strip enters the annealing unit. The chemical composition of the steel substrates and the thickness and the coating weight of the zinc-coated steel sheets are given in Tables 1 and 2.

Galvannealing experiments were performed on the zinc-coated samples of 30 × 170 mm using Gleeble 3500 thermo-mechanic physical simulator, where the samples were heated and cooled using a high-speed resistive heating and an air cooling unit to simulate the industrial galvannealing process. The annealing temperatures were pre-set as 480, 500, 520, 540, and 560°C, and annealing times as 5, 10, 20, 40 s to bring out the effect of main process parameters on the coating properties. A high heating rate of 400°C/s was used on the zinc-coated samples to heat from room temperature to the pre-set annealing temperatures to avoid any transformation that might occur in the coting during heating and to simulate the onset conditions of the withdrawn steel sheet at the exit of liquid zinc bath. After each dwell time at the specified annealing temperature, samples were first cooled down to 350°C with an average cooling rate of 35 °C/s using an air jet, subsequently further cooled to 200°C, and then to room temperature with average cooling rates of 5 °C/s and 35 °C/s respectively. Subsequent examinations and analyses were carried out in the middle portion of the samples, where the temperature difference was ±3°C.

The surface roughness value Ra of the coatings was measured with Mahr Perthometer M2 surface roughness tester. A stock solution was prepared by dissolving 2.1 g hexamethylenetetramine in 300 ml HCl, and then water added into this solution until a 2-lt solution was obtained to determine the iron content of galvannealed coatings. The coating layer in an area of 20 × 30 mm on the sample surface was dissolved using the solution until no gas bubble release was observed. Afterward, the iron content was determined using Spectro Ciros CCD inductively coupled plasma spectrometer.

The morphological variations on the coating surfaces were observed through Jeol JSM 5600 scanning electron microscope (SEM). The identification of each phase was accomplished with the help of their distinct morphological characteristics viz. pillar for ζ, granular for δ_{1p}, faceted for δ_{1k} [17-20]. The phases in the as-received and thoroughly treated samples were identified using Rigaku D/MAX-2200 Ultima + X-ray diffractometer equipped with Cu target. The operating conditions were 50 kV and 1000 μA, and the data were collected using Cu-Kα radiation (λ = 1.5405 Å) between 30° and 50° in 2θ.

TABLE 1

Chemical composition of the steel substrates (wt.%)

Steel substrate	C	Mn	Si	S	P	Al	Ti	Nb	N
AK	0.030	0.140	0.012	0.008	0.006	0.053	—	—	0.0040
IF	0.003	0.070	0.006	0.004	0.005	0.032	0.025	0.010	0.0035

TABLE 2

Thickness of the steel substrates and weight of the zinc-coatings

Steel substrate	Thickness of the steel substrate (mm)	Weight of the zinc coating (g/m^2 on each side of the steel sheet)
AK	0.74	66.44
IF	0.64	48.14

3. Experimental Results

The variation of the surface roughness according to steel type, annealing temperature and time is shown in Figure 2. The surface roughness of each steel coating followed a different course set by annealing temperature and time. It was found that the surface roughness increased from 1.12 to 1.37 µm in galvannealed low carbon Al-killed steel (GAKS) while it decreased from 1.12 to 0.83 µm in galvannealed Ti-Nb stabilized interstitial free steel (GIFS).

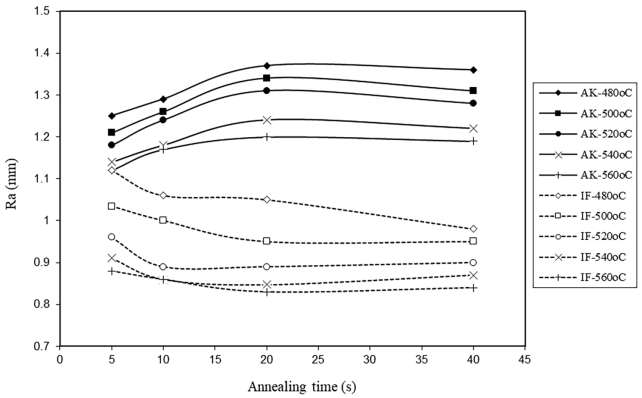

Fig. 2. Variation of Ra in GAKS and GIFS with annealing temperature and time

The change in iron content of the galvannealed coatings with annealing time and temperature brought out the effect of the chemical composition of the steel substrates on the reaction kinetics of Fe-Zn phases (Fig. 3). Due to the rather low alloying content of IFS, the iron content of the GIFS reached an exponential value relatively faster than that of GAKS.

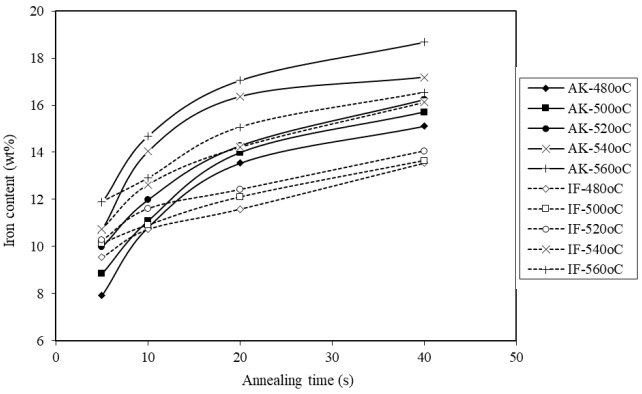

Fig. 3. Effect of annealing temperature and time on the iron content of GAKS and GIFS

The coatings on the as-received samples displayed a solidified pure zinc structure. In XRD analysis, none of the known Fe-Zn phases were identified in the as-received samples, which is evidence of unalloying (Fig. 4). From the early moments of the galvannealing process, the crystalline structures that appeared on the coating surface of both steel samples indicated an alloying from the Fe-Zn interface to the coating surface (Figs 5 and 6). Many crater formations, the numbers, and the sizes of which

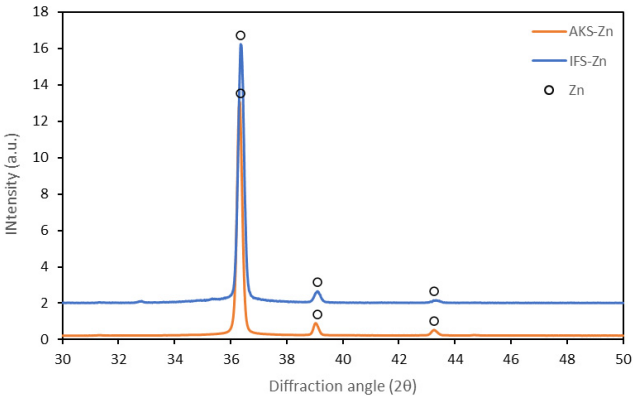

Fig. 4. XRD pattern of the as-received zinc-coated samples

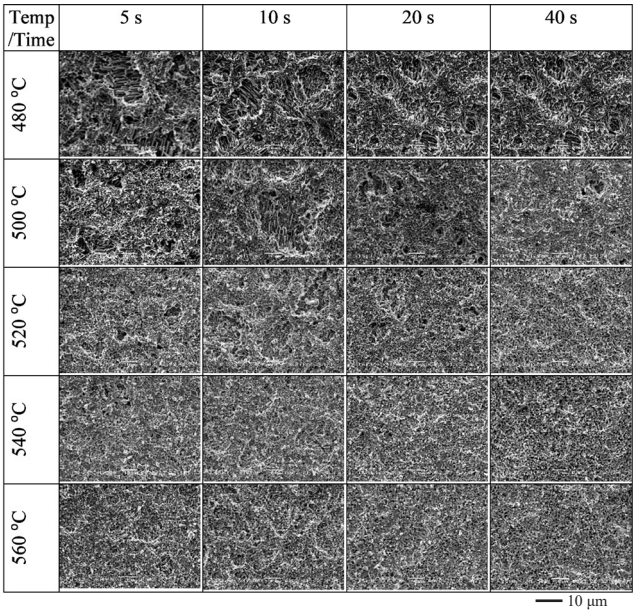

Fig. 5. Surface microstructures of GAKS using SEM, resulting from different galvannealing cycles

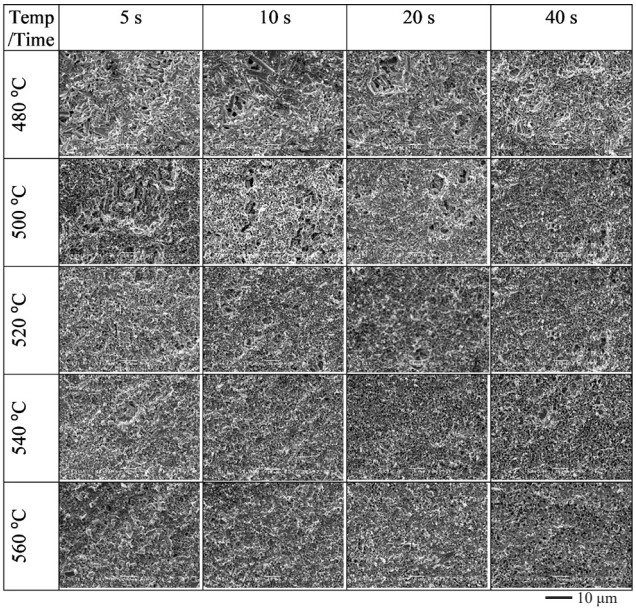

Fig. 6. Surface microstructures of GIFS using SEM, resulting from different galvannealing cycles

generally decrease with increasing of annealing temperature and time were observed on the coating surfaces of AKS and IFS.

The pillar type ζ crystals were located alone in the craters while there was a mixture of pillar ζ and granular type δ_{1p} crystals outside of the craters (Fig. 7a,b). As the temperature and time increased, the proportion of these crystals in the mixture changed, and the δ_{1p} crystals became dominant at higher annealing temperatures and for longer annealing times. Although most of the crystals at elevated temperatures were formed by δ_{1p} crystals, in some areas, the faceted δ_{1k} crystals were encountered (Fig. 8). All of these Fe-Zn phases were detected in the samples fully annealed at 560 °C through an XRD analysis (Fig. 9).

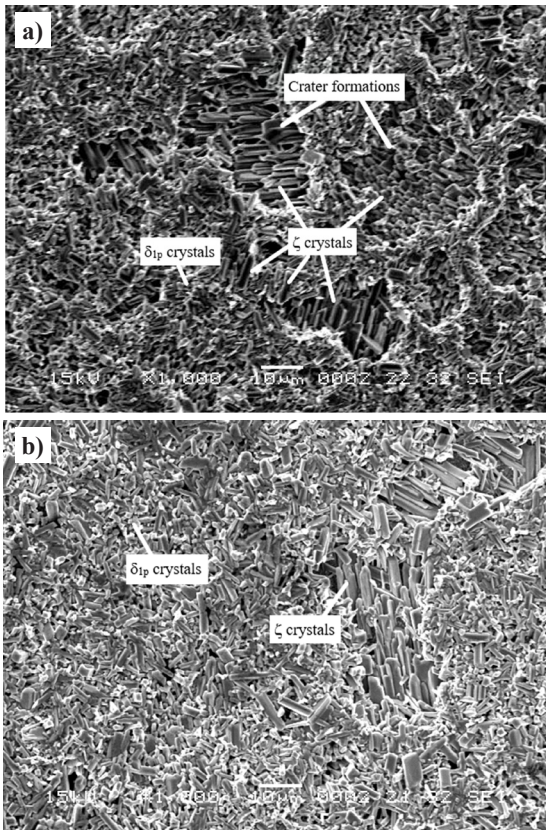

Fig. 7. Alloyed coating surfaces of (a) AKS and (b) IFS after 5 s annealing at 480°C

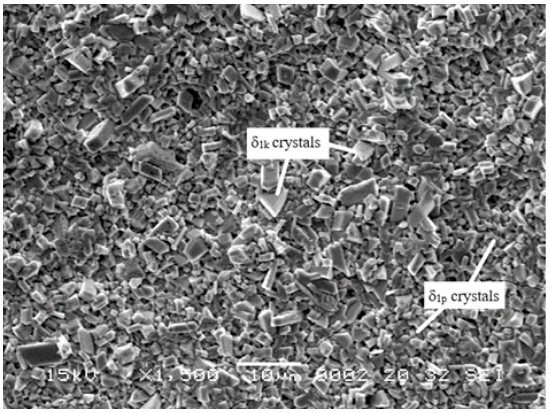

Fig. 8. δ_{1p} and δ_{1k} crystals observed on the surface of GIFS after 5 s annealing at 560°C

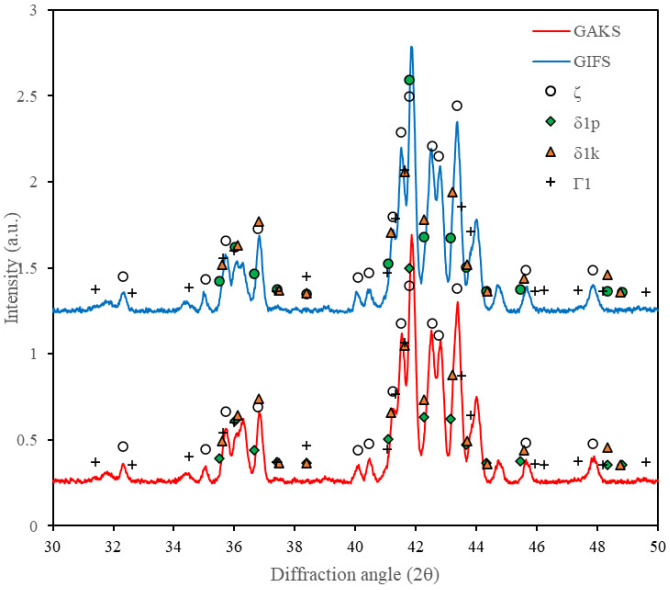

Fig. 9. XRD analysis of the fully annealed samples

4. Discussion

The galvannealing process promotes the diffusive growth of iron-containing phases into the zinc layer to form a galvannealed coating. As this growth is nonuniform, it forms craters in the coating layer [21]. The craters scattered randomly on the galvannealed coatings lead to significant changes in surface roughness by generating thickness fluctuations. They have a relatively large size in low-temperature annealing cycles, and their size decreases with increasing of annealing temperature and time. Hale et al. [22] were reported that there are clear correlations between increased crater density and reduced powdering and improved paint adherence.

Based on the SEM images taken from the samples annealed at 520°C and below, the coating surfaces had randomly scattered craters composed of pillar type ζ crystals. The ζ crystals were disappeared with increasing temperature, and no ζ crystal was observed above 520°C. This result complies with the explanation of Inagaki et al. [23], reporting that the peritectic transformation temperature of ζ phase is 530°C and ζ phase disappears above this temperature. As seen in Figure 8a and 8b, the existence of oriented crystals confirms the model of epitaxial growth proposed by Carless et al. [24]. According to this model, the oriented crystals accommodate upon the preferentially {111} oriented α-Fe grains and create a stable barrier for the diffusion of Fe-Zn phases while regular progress is proceeding to surround it.

Due to the different chemical compositions of AKS and IFS substrates, the evolution of surface roughness in GAKS and GIFS exhibits different characteristics with annealing temperature and time. Although the surface roughness of both steel coatings shows an exponential behaviour with increasing of annealing time, it is in increasing order in GAKS, vice versa in GIFS (Fig. 2). However, in both steel coatings, there is a decreasing trend in surface roughness with increasing of annealing temperature. The higher Ra values of both steel coatings are associated with

crater formations, which is more significant in GAKS. Upon disappearing of the craters, the change in Ra values decreases. This alteration can be explained by the complete depletion of ζ phase at the surface and its replacement with δ_1 phases. The lower surface roughness of GIFS was thought to be associated with the higher reactivity of IFS substrate. As the shortest annealing time in the experiments was 5 s, the surface roughness of GIFS for the shorter periods of time could not be identified. It is assumed that the crater formations in GIFS were completed in less than 5 s due to the relatively high reactivity of IFS [3,18]. This explains how the ζ phase in the GIFS surface was depleted in a short period of time, and how the surface was coated solely with δ_1 phases.

The change in the surface roughness can also be explained by the iron content of the coatings. In general, the surface roughness decreases with the increasing iron content of both steel coatings, depending on the temperature (Fig. 10). However, the surface roughness shows different behaviour with respect to annealing time at each temperature depending on the type of steel substrate that influences the reaction rate in the coating, as described above.

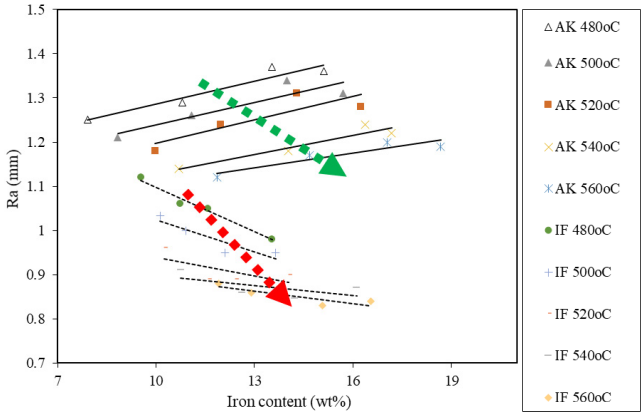

Fig. 10. Surface roughness of the coatings associated with iron content (dashed red and green arrows show IFS and AKS coatings respectively)

5. Conclusions

The findings of this study can be summarized as follows:

- Surface roughness follows a decreasing trend with increasing of annealing temperature in both steel coatings.
- However, surface roughness exhibits an exponential behaviour with increasing of annealing time at each annealing temperature, which is in an increasing order in GAKS, vice versa in GIFS.
- The chemical composition of the steel substrates has a significant effect on the surface roughness of the coatings, which can be explained by the faster evolution of Fe-Zn phases in GIFS compared to GAKS.
- Crater formations significantly increase surface roughness, which is more significant in GAKS.
- An increase in the iron content of the coatings leads to a reduction in the surface roughness with the formation of cubic δ_{1k} phase.
- Surface roughness can be used as fast feedback for the adjustment of galvannealing parameters.

REFERENCES

[1] T. Irie, Developments of zinc-based coatings for automotive sheet steel in Japan, in: G. Krauss, D. Matlock (Eds.), Zinc-Based Steel Coating Systems: Metallurgy and Performance, TMS/AIME, Warrendale, PA, USA (1990).
[2] Y. Hisamatsu, Proc. 1st Int. Conf. on Zinc and Zinc Alloy Coated Steel Sheet (Galvatech'89), ISIJ, Tokyo, Japan (1989).
[3] A.R. Marder, Prog. Mater. Sci. **45**, 191-271 (2000).
[4] N. Bandyopadhyay, G. Jha, A.K. Singh, T.K. Rout, N. Rani, Surf. Coat. Tech. **200**, 4312-4319 (2006).
[5] M.A. Ghoniem, K. Lohberg, Metall. **26** (10), 1026-1030 (1972).
[6] O. Kubaschewski, Iron-Binary Phase Diagrams, Springer-Verlag Berlin Heidelberg GmbH, Aachen, Germany (1982).
[7] J. Nakano, D.V. Malakhov, G.R. Purdy, Calphad, **29** (4), 276-288 (2005).
[8] R. Kainuma, K. Ishida, Tetsu To Hagane **91**, 349-355 (2005).
[9] G. Beranger, G. Henry, G. Sanz, The Book of Steel, Lavoisier Publishing with the participation of SOLLAC-Usinor Group, Paris, France (1996).
[10] T. Nakamori, Y. Adachi, T. Toki, A. Shibuya, ISIJ Int. **36** (2), 179-186 (1996).
[11] I. Hertveldt, B.C. De Cooman, J. Dilewijns, 39th MWSP Conference Proceedings, ISS-AIME, ISS, Indianapolis, IN, USA (1997).
[12] M. Chida, H. Irie, U.S. Patent Number 10,597,764 B2 (2020).
[13] S. Sriram, V. Krishnardula, H. Hahn, IOP Conf. Ser-Mat. Sci. **418** (1), 012094 (2018).
[14] M. Sakurai, J.I. Inagaki, M. Yamashita, Tetsu-to-Hagane, **89** (1), 18-22 (2003).
[15] S. Sepper, P. Peetsalu, M. Saarna, Agron. Res., Special Issue **1**, 229-236 (2011).
[16] K.I.V. Vandana, M. Rajya Lakshmi, Int. J. Innov. Eng. Tech. **5** (2), 359-363 (2015).
[17] M. Urai, M. Arimura, M. Terada, M. Yamaguchi, H. Sakai, S. Nomura, Tetsu To Hagane **43** (19), 27-30 (1996).
[18] C.S. Lin. M. Meshii, C.C. Cheng, ISIJ Int. **35** (5), 503-511 (1995).
[19] F.E. Goodwin, T. Indian I. Metals **66**, 5-6 (2013).
[20] G. Moréas, Y. Hardy, Rev. Met. Paris **98** (6), 599-606 (2001).
[21] A. van der Heiden, A.J.C. Burghardt, W. van Koesveld, E.B. van Perlstein, M.G.J. Spanjers, Galvanneal Microstructure and Anti-Powdering Process Windows, in: A.R. Marder (Ed.), The Physical Metallurgy of Zinc Coated Steel, TMS/AIME Conf. Proc., San Francisco, CA, USA (1994).
[22] P.M. Hale, R.N. Wright, F.E. Goodwin, SAE Technical Paper 2001-01-0084, 2001.
[23] J. Inagaki, M. Sakurai, T. Watanabe, ISIJ Int. **35** (11), 1388-1393 (1995).
[24] S.P. Carless, G.A. Jenkins, V. Randle, Ironmak. Steelmak. **27** (1), 69-74 (2000).